BNL-212408-2019-JAAM

Interface-confined triangular FeOx nanoclusters on Pt(111)

Z. Zhou, P. Liu

To be published in "The Journal of Chemical Physics"

December 2019

Chemistry Department

Brookhaven National Laboratory

U.S. Department of Energy

USDOE Office of Science (SC), Basic Energy Sciences (BES) (SC-22)

DISCLAIMER

The Journal of Chemical Physics

Interface-confined triangular FeO_x nanoclusters on Pt(111)

Zhiwen Zhou,[1,2] Ping Liu,[3*] Fan Yang,[1*] and Xinhe Bao[1]

AFFILIATIONS

[1] State Key Laboratory of Catalysis, Dalian Institute of Chemical Physics, Chinese Academy of Sciences, Dalian 116023, China

[2] University of Chinese Academy of Sciences, Beijing 100049, China

[3] Chemistry Division, Brookhaven National Laboratory, Upton, New York 11973, United States

[*] Author to whom correspondence should be addressed: pingliu3@bnl.gov; fyang@dicp.ac.cn

ABSTRACT

Under the oxidizing condition, the cheap metal component of bimetallic catalysts often segregates to the surface and form oxide nanoclusters (NCs) supported on the metal surface, which exhibit unique structures and catalytic properties drastically different from the corresponding bulk materials. Here, density functional theory (DFT) calculations are employed to describe the atomic and electronic structures of a series of triangular FeO_x NCs confined on Pt(111) with the size ranging from ~ 0.3 nm to ~ 2.2 nm, which behave differently from the FeO film reported previously. The lattice of supported FeO_x NC on Pt(111) is found to vary not only with the NC size, but also with the Fe/O ratio or the edge termination. Owing to a strong FeO_x-Pt interaction, the heterogeneous distribution in local atomic and electronic structures of Fe across the FeO_x NC is observed, though each Fe is positioned at the three-fold hollow site of Pt(111). Our study not only sheds light on the catalytically active sites of supported FeO_x NCs, but also provides guidance for the design of highly active and stable oxide nanocatalysts under reactive environment.

I INTRODUCTION

Supported nanoclusters (NCs) exhibit chemical properties drastically different from bulk materials and are of tremendous importance for catalysis and energy related technologies.[1, 2] The finite size effect of metal NCs in their electronic structures and chemical properties have been widely studied in the past two decades.[3-6] The combination of electronic/geometric effects and structural fluxionality of NCs together with the synergy of NCs and supports at the interface may allow the breaking of scaling relationships at atomic scale and exhibit unique chemical properties during chemical reactions.[6-8] Despite the potential application of metal oxide NCs in catalysis,[9, 10] the mechanistic understanding at the atomic level is limited and remains elusive.

FeO nanostructures (NSs) supported on Pt(111) (labeled as FeO-Pt) have been reported as active catalysts for a number of catalytic processes, e.g. the preferential oxidation of CO (PROX)[11], the selective oxidation of primary alcohols[12], and the water-gas-shift (WGS) reaction.[13] During PROX, the interface-confined coordinatively unsaturated Fe (CUF) centers at the edge of FeO_x NSs have been identified as the active centers both experimentally and theoretically.[11, 14, 15] The dynamic size effect of FeO-Pt, especially for FeO_x NCs with size below 3 nm, has also been demonstrated recently by scanning tunneling microscopy (STM) study for the transition from the CUF edge to coordinatively unsaturated O (CUO) edge under oxidative atmosphere.[16, 17] While considerable efforts were devoted to investigate the atomic and

electronic structure of the FeO film on Pt(111), little attention has been paid for the catalytically active FeO_x NCs.[18-23]

Here, we employ density functional theory (DFT) to study the interface-confined small FeO_x NCs on Pt(111) from Fe_3O (~ 3 Å) to $Fe_{28}O_{36}$ (~ 22 Å). Our study describes the effects of size, Fe/O ratio or edge termination of FeO_x NCs on the corresponding binding configuration/ interfacial interaction with Pt(111) and the atomic/electronic structures. Our study brings atomic understanding to the properties of supported FeO_x NCs and opens new ways for the optimization and design of oxide nanocatalysts by controlling the oxide-metal interaction.

II COMPUTATIONAL DETAILS

Spin-polarized density functional theory (DFT) calculations were performed using the Vienna ab-initio simulation package (VASP)[24, 25]. The projected augmented wave (PAW) potentials[26] were employed with the exchange-correlation functional of Perdew, Burke and Ernzerhof (PBE)[27]. The kinetic cutoff of the plane wave set is 400 eV. The method of Gaussian smearing was adopted to set the partial occupancies for each wavefunction with the width of the smearing of 0.05 eV. The strong correlated 3d electrons of Fe were described through DFT+U method first introduced by Dudarev et al.[28] The U_{eff} (U_{eff} = U - J) of 3 eV was reported previously to successfully describe the properties of both bulk and supported iron oxides[29, 30].

According to our previous STM studies,[16, 17] small FeO_x NCs with Fe-O bilayer and approximately equilateral triangular shape were truncated from the monolayer FeO(111) slab by adopting the CUF edge or the CUO edge (denoted as CUF or CUO NCs for short, Schematic 1). Both CUF NCs (Fe_3O, Fe_6O_3, $Fe_{10}O_6$, $Fe_{15}O_{10}$, $Fe_{21}O_{15}$, $Fe_{28}O_{21}$) and CUO NCs (Fe_3O_6, Fe_6O_{10}, $Fe_{10}O_{15}$, $Fe_{15}O_{21}$, $Fe_{21}O_{28}$, $Fe_{28}O_{36}$) were deposited on a 3-layer Pt(111) slab with the optimized Pt-Pt bulk distance of 2.806 Å, where the bottom two layers were constrained and the top layer was allowed to relax with the interacted FeO_x NCs during structural optimization until the residual forces were less than 0.02 eV/Å. The 6×6 and 10×10 Pt(111) arrays were used as the substrate for Fe_3O_x/Fe_6O_x and larger NCs, respectively. The vacuum layer of ~12 Å was selected. The Γ-centered k-mesh sampling in Brillouin zone of 2×2×1 and Γ-point were considered for 6×6 slab and 10×10 slab, respectively. The oxidation states were obtained through normalized Bader Charge analysis.[31] To describe their magnetic properties, we arranged the magnetic structure as row-wise (RW-AFM) ordering according to the studies by Giordano et al.;[30] however, for maintaining the approximately equal amount of Fe atoms with opposite magnetic moment, we aligned the opposite magnetization evenly for the extra row (the bottom most row of Fe for each NC in Fig. 1). To assure whether the AFM ordering is stable for FeO_x NCs, we compared the total energy difference between the ferromagnetic (FM) and the AFM ordering (ΔE) for CUF and CUO NCs of different sizes (Table I). Since ΔE is always positive in Table I, we can conclude that in line with Pt(111) supported FeO film,[30] small FeO_x NCs are also apt to adopt the AFM ordering. The stabilization in energy via AFM ordering is ~ 0.16 eV per Fe more significant for the CUO NCs as compared to that via the FM ordering. While for the CUF NCs, such stabilization becomes weaker. Accordingly, for all FeO_x NCs studied here, the AFM orderings were applied. We also tested the effect of dispersion correction on $Fe_{10}O_{15}$/Pt(111) using PBE-D3.[32] The results show that including the dispersion forces results in the slight expansion of lattice, and the corresponding distribution within the NC, which is the interest here, remains the same.

III RESULTS AND DISCUSSION

A. Adsorption configuration of FeO_x on Pt(111)

Due to the lattice mismatch between FeO and Pt, three high-symmetry domains (fcc, hcp, top) have been

observed for the film or large islands of FeO by STM[17, 23] or theoretical modelings,[30, 33] depending on the position of Fe adsorption sites on Pt(111). The FeO_x NCs with size smaller than the Moire pattern (~ 26 Å[18-20, 23], observed for films and large islands) likely adjust their lattice to match well with Pt(111) due to the strong interaction with Pt(111) and structural fluxionality, i.e. each NC only exhibits one domain. Our calculations show that the top site is extremely unstable for FeO_x NCs, which shift away from top site during the structural optimization. Thus, only four types of configuration were included in the current calculation, i.e., Fe at fcc site / O over hcp or top site, Fe at hcp site / O over fcc or top site. To estimate the stability of a FeO_x NC, the relative total energy (ΔE_{tot}) was calculated via $\Delta E_{tot}=\frac{(E_{tot}-E_{ref})}{N_{Fe}}$, where E_{tot} is the total energy of FeO_x/Pt(111), E_{ref} is the total energy of the one of configurations for each FeO_x/Pt(111, and N_{Fe} is the number of Fe in the corresponding FeO_x NC. The more positive ΔE_{tot} corresponds to the less stable configuration.

TABLE I. Totally energy differences for FeO_x NCs on Pt(111) of different magnetic structures.

Number of Fe in FeO_x NC	[a]ΔE (CUF) eV per Fe	[a]ΔE(CUO) eV per Fe
3	0.03	0.14
6	0.04	0.17
10	0.05	0.16
15	0.07	0.18
21	0.09	0.16
28	0.10	0.17

[a]$\Delta E= (E_{FM} – E_{AFM})/N_{Fe}$, where E_{FM} and E_{AFM} are the DFT-calculated total energies of the NC with FM and AFM orderings, respectively; N_{Fe} is the number of Fe atoms of a FeO_x NC.

CUF NCs on Pt(111). All CUF NCs of FeO_x studied here match well with the lattice of Pt(111) support via solely Fe-Pt bonds, where the O-coordination numbers of Fe atoms range from 1 to 3 depending on their corresponding location in the NC, i.e., from corner, edge to center and the Fe-coordination number of O is uniformly 3 (Fig. 2). Our results clearly show that the energetically favored binding sites for Fe_3O, Fe_6O_3 and $Fe_{10}O_6$ NCs correspond to those with Fe atoms anchored at the fcc sites and O atoms located over the hcp sites of Pt(111) (Fig. 2a,e,i). By comparison, the configuration with Fe at the Pt hcp site and O over the Pt fcc site is slightly less stable by 0.03 or 0.04eV per Fe (Fig. 2c,g,k), while those with O over the Pt top site are least stable with ΔE_{tot} of 0.07 ~ 0.11eV per Fe (Fig. 2b,d,f,h,j,l). That is, to stabilize the FeO_x NC, both Fe and O atoms should be positioned over the high symmetric hollow sites. Additionally, when going from Fe_3O (Fig 2a-d) to Fe_6O_3 (Fig. 2e-h) and $Fe_{10}O_6$ (Fig. 2i-l), ΔE_{tot} of the corresponding configuration is almost the same, indicating that for CUF NCs, size effect on the adsorption configuration is small.

CUO NCs on Pt(111). The adsorption of CUO NCs on Pt(111) are more complicated than the case of CUF NCs. The adsorption configuration with Fe atoms at the Pt hcp site was not considered in this case due to the lower stability as compared to those at the Pt fcc sites (Fig. 2). For CUO NCs, the O-coordination numbers of Fe atoms are at least 2, while the Fe-coordination numbers of O atoms range from 1 to 3 (Fig. 3). Going from 3-coordinated O atoms at the center, 2-coordinated O atoms at the edge to 1-coordinated O atoms at the corner, the corresponding CUO NC shows increasing ability to interact directly with the substrate Pt and fluxionality to adjust itself and strengthen the CUO-Pt(111) interaction (Fig. 3). Thus, although the positions of O atoms greatly affect the stability of CUO NCs on Pt(111) as observed for the CUF NCs (Fig. 3), the trend is opposite (Fig. 2). For Fe_3O_3 NC, the adsorption with O over the top site of Pt(111) (Fig. 3b) is more stable than that with O over the Pt hcp site (Fig. 3a) by 0.13eV per Fe. The preferential adsorption to the site with O over the Pt top site of Pt(111) is attributed to the presence of active 2-coordinated O atoms at the edge.

In this case, 33% of O atoms are active enough to shift downward toward Pt(111) and form Pt-O bonds with the underneath Pt atom (Fig. 3b), which is not the case for O atoms over the hcp sites of Pt(111) (Fig. 3a). Similar situation is also observed for Fe_3O_6 NC. Due to the presence of additional single-coordinated O atoms at the corner, the stability gain of -0.26 eV per Fe is reached by shifting O form the hcp to the top of Pt(111) (Fig. 3d). Although the binding motif for corner O over the Pt hcp site also involves the Pt-O bond formation (Fig. 3c), the corresponding bond length (d_{Pt-O} = 2.100, 2.068 Å, bridge site) is longer than that over the Pt top site (d_{Pt-O} = 1.959 Å, Fig. 3d). In addition, the ratio of active O involved in Pt-O bond formation is also smaller (50% for O over hcp vs. 67% for O over top), and thus the weaker stabilization of Fe_3O_6 NC on Pt(111) is observed.

Fe_6O_x NCs behave similarly as Fe_3O_x NCs, where the site with O over the Pt top (Fig. 3f,h) is preferred rather than that over the hcp (Fig. 3e,g) and such preference is more significant for Fe_6O_{10} (ΔE_{tot} = -0.08 eV per Fe) than Fe_6O_7 (ΔE_{tot} = -0.03 eV per Fe). Again, this is associated with active O atoms which are only observed at the edge or corner sites of each NC (Fig. 3). However, with the size increasing from Fe_3 to Fe_6, the magnitude for preferential adsorption with O over the Pt top site decreases. In the case of $Fe_{10}O_x$, the $Fe_{10}O_{12}$ still favors O atoms over top sites of Pt(111) (ΔE_{tot} of -0.04 eV per Fe, Fig. 3i,j), while for $Fe_{10}O_{15}$, the adsorption configuration with O over the Pt hcp site is favored (ΔE_{tot} = 0.02 eV per Fe, Fig. 3k,l).

According to DFT calculations, there are two factors to determine the preferential site of FeO_x on Pt(111). One is the stacking sequence of Fe-O bilayer on Pt(111); the other is the ratio of active O atoms in FeO_x NC which can interact directly with Pt. Without the presence of active O atoms, e.g. CUF NC, the favorable adsorption site only depends on how the Fe and O are stacked at the Pt-Fe-O interface. The stacking sequence following that of Pt(111) is always preferred with both Fe and O over the hollow sites of Pt (Fig. 2). With the presence of active O atoms, e.g. CUO NCs including $Fe_3O_{3,6}$, $Fe_6O_{7,10}$ and $Fe_{10}O_{12}$ (Fig. 3), the adsorption favors the motif with O over the top site of Pt(111). The active O atoms are represented by the low-coordinated O atoms at the corner and edge of FeO_x NCs. The low coordination enables the flexibility of O, and the position over the top of Pt provides a the shorter path and the less distortion of local structure, as compared with those over the Pt hollow site, to enable the direct interaction between O with Pt(111). Yet, such site preference is weakened with the increase in size and thus the decrease in ratio of active O atoms. The $Fe_{10}O_{15}$ NC is likely the critical point for the site transition between the one with O over the top site of Pt(111) and that with O over the hcp site.

Following the principle above, we can now deduce the most stable adsorption site on Pt(111) for larger FeO_x NCs, which significantly decreases the computational cost. That is, for CUF NCs, $Fe_{15}O_{10}$, $Fe_{21}O_{15}$, $Fe_{28}O_{21}$ (Fig. 4a,c,e), prefer to be positioned on Pt(111) via both Fe and O over the hollow sites of Pt(111). Similar configuration is also adopted by the large CUO NCs, $Fe_{15}O_{21}$, $Fe_{21}O_{28}$, $Fe_{28}O_{36}$ (Fig. 4b,d,f), where with limited number of active O atoms at the edge and corner of the CUO NC the adsorption with O located over the top of Pt(111) is not as preferential as that over the Pt hollow site. In the following, we will take the most stable adsorption configuration of CUF and CUO NCs on Pt(111) to discuss the size and interface effects on the atomic and electronic structures by varying the size from Fe_3 to Fe_{28} together with the Fe/O ratio.

B. Atomic structure of supported FeO_x

In this session, we focus on the geometries of Fe interfacial layer in FeO_x NCs and on Pt(111). Previously, the FeO film or large FeO islands supported on Pt(111) have been found to exhibit various adsorption sites for the interfacial Fe layer, which results in different high-symmetry domains (fcc, hcp, top).[30, 33] The in-plane FeO lattice parameter (the distance between two neighboring Fe, l_{Fe} in our notation) and the interfacial lattice parameter (the spatial separation between the bottom of FeO film and Pt(111) substrate, h_{Fe} in our notation) were reported to

increase in the order of fcc < hcp < top domain.[30, 33] It seems that for FeO film the strong interaction with Pt(111) not only shortens the interfacial distance, but also makes the in-plane FeO lattice parameter contracted to match the lattice of Pt(111). However, in each domain the properties were suggested to be homogeneous.[30, 33]

Different from the FeO film, each interfacial Fe atom adopts the same adsorption sites for the small FeO_x NCs supported on Pt(111) except Fe at the corner site of CUO NC of $Fe_{10}O_{15}$ or larger NCs. While the distribution of binding motif within a FeO_x NC is heterogenous rather than homogeneous according to the calculated distribution of l_{Fe}. For the Pt(111)-supported CUF NCs (Fig. 5a-f), the overall lattice contraction was observed. The distribution pattern for l_{Fe} is mostly symmetric depending on the site geometry, where l_{Fe} decreases in the sequence: center > edge > corner for $Fe_{15}O_{10}$ and larger NCs. By comparison, such site-dependent distribution is less obvious with the decreasing of NC size (Fig. 5a-f). This is likely associated with the stronger FeO_x-Pt(111) interaction and higher structural fluxionality for the small NCs compared to the large NCs, which favor the epitaxial growth. l_{Fe} at any site turns out to be smaller than average l_{Fe} for FeO film. Compared to the lattice contraction for fcc domain of FeO film (average lattice, 3.0 Å),[30, 33] with the greater fluxionality the edge and corner of CUF NCs tend to contract the lattice in higher degree. Besides, the average l_{Fe} ($\overline{l_{Fe}}$) is also calculated (Table II, left). Except Fe_3O, the $\overline{l_{Fe}}$ increases and approaches to 3.0 Å, while mismatch with Pt(111) gets larger as the size increases to $Fe_{28}O_{21}$. It again indicates the gain in structural rigidity and the weakening in interfacial interaction introduced by increased NC size.

The Pt(111)-supported CUO NCs (Fig. 5g-l) behave differently from CUF NCs, where the overall lattice expansion is observed as compared to FeO film except for Fe_3O. In addition, the distribution of l_{Fe} along the FeO_x lattice also differs, which is asymmetric in the case of CUO NCs. Extremely large l_{Fe} values can be observed at corner site (maximum value, 3.43 Å, Fig. 5i), and the l_{Fe} at the equivalent corner or edge sites may not necessarily be the same due to the presence of active O atoms, which are directly bound to Pt and thus Fe-Fe bond is stretched in response (Fig. 5). $\overline{l_{Fe}}$ decreases as size increasing from $Fe_{10}O_{15}$ to $Fe_{28}O_{36}$ (Table II, right), which is opposite against that for CUF NCs. In this case, the gained structural rigidity and the weakened interfacial interaction with the increasing of size reduce the lattice expansion toward that of FeO film. The opposite trends are observed going from Fe_3O_6 to Fe_6O_{10}, where $\overline{l_{Fe}}$ increases with size (Table II). Like the cases of CUF, the CUO NCs with such small size enables the stronger interaction with Pt(111) and higher structural fluxionality than the big ones to match the lattice of Pt(111).

TABLE II. The average value of in-plane FeO_x lattice parameter for FeO_x NCs on Pt(111).

CUF NCs	$\overline{l_{Fe}}$ (Å)	CUO NCs	$\overline{l_{Fe}}$ (Å)
Fe_3O	2.867	Fe_3O_6	3.034
Fe_6O_3	2.850	Fe_6O_{10}	3.137
$Fe_{10}O_6$	2.906	$Fe_{10}O_{15}$	3.289
$Fe_{15}O_{10}$	2.929	$Fe_{15}O_{21}$	3.259
$Fe_{21}O_{15}$	2.930	$Fe_{21}O_{28}$	3.236
$Fe_{28}O_{21}$	2.933	$Fe_{28}O_{36}$	3.207

The different behaviors between CUF and CUO (Fig. 6) NCs supported on Pt(111) are also seen in term of relative h_{Fe} (Δh_{Fe} expressed with respect to the lowest height in each NC). In the case of CUF NCs, the Δh_{Fe} for each NC descends in the order of center > edge > corner for $Fe_{10}O_6$ and larger NCs (Fig. 6c-f). For Fe_6O_3 (Fig. 6b), Δh_{Fe} is in the order of edge > corner site, while for Fe_3O (Fig. 6a), Δh_{Fe} is almost zero since only corner site exists. That is, the corner Fe is located the most closely to Pt(111)

TABLE III. Average Fe oxidation state and magnetic moments for FeO_x NCs on Pt(111).

CUF NCs	Nominal oxidation state for FeO_x	Normalized average oxidation state for FeO_x/Pt	Average magnetic moment for FeO_x/Pt (μ_B)	CUO NCs	Nominal oxidation state for FeO_x	Normalized average oxidation state for FeO_x/Pt	Average magnetic moment for FeO_x/Pt (μ_B)
Fe_3O	+0.667	+1.459	3.556	Fe_3O_6	+4.000	+2.300	3.675
Fe_6O_3	+1.000	+1.590	3.598	Fe_6O_{10}	+3.333	+2.251	3.789
$Fe_{10}O_6$	+1.200	+1.698	3.638	$Fe_{10}O_{15}$	+3.000	+2.328	3.777
$Fe_{15}O_{10}$	+1.333	+1.772	3.660	$Fe_{15}O_{21}$	+2.800	+2.333	3.803
$Fe_{21}O_{15}$	+1.429	+1.821	3.681	$Fe_{21}O_{28}$	+2.667	+2.300	3.838
$Fe_{28}O_{21}$	+1.500	+1.854	3.694	$Fe_{28}O_{36}$	+2.571	+2.290	3.836

which is followed by edge Fe and center Fe in an increasing sequence, and thus the strongest Pt-(corner Fe) bond is formed to help stabilize the NC. By comparison, the CUO NCs demonstrate more complex Δh_{Fe} distribution patterns along the FeO_x lattice (Fig. 6g-l). Like the l_{Fe} distribution (Fig. 5g-l), the asymmetric patterns are also observed. The h_{Fe} at the center site is within the lower medium range, while the maximum and minimum h_{Fe} occur at the edges and corners (Fig. 6b-f). The emergence of extreme value of h_{Fe} is associated with the active O atoms at the edges and corners (Fig. 3), which locate closely to Pt(111) and form Pt-O bonds. As a result, Fe atoms connected to active O atoms are forced to move downward toward Pt(111) and thus the minimum h_{Fe} is observed, while at meanwhile the neighboring Fe atoms are pushed in opposite direction and leads to the maximum h_{Fe}.

The predictions from our DFT calculations well explain the previous microscopic measurements. First of all, the STM only observes one main orientation for each FeO_x/Pt(111).[17, 23] Indeed, the current DFT calculations show that NC always thermodynamically prefers to adopt one conformation (Fig. 2-4), in particular for the large NCs. This is associated with the large preference in in stacking sequence of both Fe and O over the hollow sites of Pt following that of Pt(111). Besides, the predicted preference of Fe to the fcc site rather than hcp site for CUF NCs (Fig. 2) was also observed by STM.[16, 17] Finally, the significantly compressed lattice at the corner (Fig. 5) likely results in the destabilization of corner Fe and facilitates the breakage of Fe-Fe bonds, which explains well the missing corner site captured experimentally.[16, 17]

Overall, for each CUF or CUO NC, the distributions of both l_{Fe} (Fig. 5) and h_{Fe} (Fig. 6) along the FeO_x lattice are heterogenous, which depends on the location of the atoms i.e., corner, edge and center site. For a CUF NC, the distribution is mostly symmetric, and the corresponding values decrease in the sequence: center > edge > corner for $Fe_{15}O_{10}$ and larger NCs. In addition, the size of NC also matters, where the impact is more significant for Fe_3O than the larger ones. With the size increasing, the area with l_{Fe} approaching or even greater than 3.0 Å (average lattice parameter of fcc domain of FeO film on Pt(111)[30, 33]) increases. The increase of l_{Fe} with NC size is also seen at the edge (very obvious for Fe_6O_3 to $Fe_{10}O_6$, not obvious from $Fe_{10}O_6$ to $Fe_{21}O_{15}$, no increase or maybe decrease from $Fe_{21}O_{15}$ to $Fe_{28}O_{21}$), while the size effect on the corner is much smaller, which is associated the lower coordination and higher flexibility to maintain the lattice contraction and thus stabilize the NC. For CUO NCs, the lattice of interlayer Fe is deeply affected by the interaction of active O at the edge and corner of NC with Pt(111),

which results in a distribution patterns for both l_{Fe} and h_{Fe} different from those of CUF NCs.

C. Electronic structure of supported FeO_x

The average oxidation states of Fe for FeO_x NSs (Table III) are calculated and normalized based on the Bader Charge analysis with respect to bulk Fe, FeO and Fe_2O_3. The metallic Fe (bcc) is used to as the reference for Fe^0 (oxidation state without normalization of 0), while the Fe ions in type-II AFM FeO (oxidation state without normalization of +1.343) and Fe in AFM α-Fe_2O_3 (oxidation state without normalization of +1.757) are considered for the standard Fe^{2+} and Fe^{3+}, respectively.

For CUF NCs (Table III, left), the Fe/O ratio is higher than 1, where Fe should be less oxidized than that of FeO. Indeed, as the size increases, the Fe/O ratio decreases from 3.000 to 1.333, while the nominal oxidation states of Fe in the unsupported CUF NCs (+0.667 to +1.500) and the normalized Fe oxidation states for the supported CUF NCs (+1.459 to +1.854) increase; yet the values for the supported NCs are still lower than +2 and the variation with Fe/O ratio is much lower than that of the unsupported. Our results clearly show that the oxidation state of Fe is significantly affected by Fe/O ratio. The interaction with Pt(111) enables the electron transfer, as demonstrated in previous study.[34] Due to the low Fe oxidation state for CUF, the electron transfer is from CUF to Pt(111), which leads to a higher oxidation state than that without Pt(111) support. In addition, the electronic modification due to the interaction with Pt(111) also decreases the sensitivity in the Fe oxidation state to the Fe/O ratio. For the CUO NCs the ratio of Fe/O is lower than 1, and thus Fe should be more oxidized than FeO. Our results show (Table III, right) that both the Fe oxidation state for the unsupported and the average value for the supported are higher than +2. With the increasing of size and Fe/O ratio from 0.500 to 0.778, the oxidation state of Fe decreases from +4.000 to +2.571 for the unsupported. When deposited on Pt(111), the Fe oxidation state remains at ~ +2.300, only slightly smaller than previous results on the FeO film on Pt(111).[33] It means that the electron transfer is from Pt to CUO. As a result, the dependence of the Fe oxidation state on the Fe/O ratio is again greatly decreased as the case of CUF. Our results clearly show that compared to the unsupported NCs, the electron transfer between FeO_x and Pt(111) tunes the Fe oxidation states for both CUF and CUO to be less sensitive to the variation in Fe/O ratio and remains at +2, which agrees well with previous experimental studies.[11, 18] In term of distribution of Fe oxidation state along a FeO_x lattice (Fig. 7), our results show that the pattern is almost same as that of h_{Fe}, where the lower h_{Fe} enables the more significant $FeO_x \leftrightarrow$ Pt electron transfer and likely stronger bonds with Pt(111).

The average local magnet moments of Fe for CUF and CUO are also calculated (Table III), which increase (from 3.556 to 3.694 μ_B for CUF; from 3.675 to 3.836 μ_B for CUO) with the increase in NC size and nominal oxidation state of Fe. In addition, the Fe magnetic moment for CUO is higher than that for the corresponding CUF with the same number of Fe atoms. Most importantly, for all supported NCs, the magnetic moment is closer to that of Fe in bulk FeO (3.610 μ_B) than that of bulk Fe (2.236 μ_B) or Fe_2O_3 (4.126 μ_B). It indicates that the oxidation states of Fe for supported NCs should be around +2, in consistent to the oxidation state analysis.

According to the DFT calcualtions, the strong FeO_x-Pt(111) interaction can enable the additional tuning to the oxidation state and thus the chemical properties of Fe atoms besides the typical variation in Fe/O ratio. Pt(111) can act as a reservoir to accept or donate electrons on interaction with FeO_x NCs. As a result, the reduced Fe, which is catalytically active, can be stabilized at the corner and edge sites of a FeO_x NC with very low Fe/O ratio). Thus, the high catalytic activity is enabled via the reduced Fe at corner and edge sites of FeO_x NCs, while the stability of NC can still be maintained due to the highly O-coordinated Fe atoms and the strong interaction with Pt(111).

IV CONCLUSIONS

DFT calculations are carried out to study the atomic and electronic structures of a series of triangular FeO_x NCs confined on Pt(111) with size ranging from ~ 0.3 nm to ~ 2.2 nm. Similar to the FeO film on Pt(111), the spin distribution based on RW-AFM ordering exhibit superior stability over FM ordering for all FeO_x NCs studied.

FeO_x NCs on Pt(111) also demonstrate unique interface-confined properties, which are very different from the film. The stable adsorption site on Pt(111) for FeO_x NCs with different size uniformly corresponds to that with Fe anchored at the Pt fcc site, while O prefers to locate over hcp site or top site depending on the edge-termination of FeO_x NCs (CUF vs. CUO) or size. For an individual FeO_x NC supported on Pt(111), the distribution in local binding motif and oxidation states of Fe is heterogeneous depending on the corresponding location in the NC, i.e, center, edge and corner. The distribution pattern also varies with the NC size, Fe/O ratio and the edge termination, which is more significant for Fe_3O_x/Fe_6O_x than for larger NCs.

Finally, the interface-confined atomic and electronic properties open new possibilities to design oxide nanocatalysts. In this case, due to the strong FeO_x-Pt interaction, the reduced Fe, which are catalytically active, can is confined at the interfacial edge or corner sites of a FeO_x NC with very low Fe/O ratio. Thus, supported oxide NCs, which are both active and stable under reactive conditions, can be achieved.

ACKNOWLEDGMENTS

This work was financially supported by Ministry of Science and Technology of China (2017YFB0602205), International Partnership Program of Chinese Academy of Sciences (121421KYSB20150016), National Science Foundation of China (91545204). P.L. would like to thank the support the U.S. Department of Energy (DOE), Office of Science, Office of Basic Energy Sciences, Division of Chemical Sciences, Biosciences and Geosciences, under contract No. DE-SC0012704.

REFERENCES

[1] Y. Li, and G. A. Somorjai, Nano Lett. **10** (2010) 2289.

[2] E. C. Tyo, and S. Vajda, Nat. Nanotechnol. **10** (2015) 577.

[3] H. Masatake *et al.*, Chem. Lett. **16** (1987) 405.

[4] M. Valden, X. Lai, and D. W. Goodman, Science **281** (1998) 1647.

[5] J. Kleis *et al.*, Catal. Lett. **141** (2011) 1067.

[6] B. Zandkarimi, and A. N. Alexandrova, J. Phys. Chem. Lett. **10** (2019) 460.

[7] H.-G. Boyen *et al.*, Science **297** (2002) 1533.

[8] Z. Xia *et al.*, J. Phys. Chem. C **123** (2019) 2182.

[9] J. B. Park *et al.*, J. Am. Chem. Soc. **132** (2010) 356.

[10] F. Jiao *et al.*, Science **351** (2016) 1065.

[11] Q. Fu *et al.*, Science **328** (2010) 1141.

[12] G. Zhao *et al.*, Nat. Commun. **8** (2017) 14039.

[13] L. Xu *et al.*, Phys. Chem. Chem. Phys. **15** (2013) 12068.

[14] D. Sun *et al.*, J. Phys. Chem. C **116** (2012) 7491.

[15] W. Kudernatsch *et al.*, ACS Nano **9** (2015) 7804.

[16] Y. Liu *et al.*, Nature Communications **8** (2017) 14459.

[17] Y. Liu *et al.*, ACS Nano **11** (2017) 11449.

[18] G. H. Vurens, M. Salmeron, and G. A. Somorjai, Surf. Sci. **201** (1988) 129.

[19] Y. J. Kim *et al.*, Phys. Rev. B **55** (1997) R13448.

[20] M. Ritter, W. Ranke, and W. Weiss, Phys. Rev. B **57** (1998) 7240.

[21] W. Ranke, M. Ritter, and W. Weiss, Phys. Rev. B **60** (1999) 1527.

[22] E. D. L. Rienks *et al.*, Phys. Rev. B **71** (2005) 241404.

[23] H. Zeuthen *et al.*, ACS Nano **9** (2015) 573.

[24] G. Kresse, and J. Hafner, Phys. Rev. B **47** (1993) 558.

[25] G. Kresse, and J. Furthmüller, Phys. Rev. B **54** (1996) 11169.

[26] G. Kresse, and D. Joubert, Phys. Rev. B **59** (1999) 1758.

[27] J. P. Perdew, K. Burke, and M. Ernzerhof, Phys. Rev. Lett. **77** (1996) 3865.

[28] S. L. Dudarev *et al.*, Phys. Rev. B **57** (1998) 1505.

[29] G. Rollmann *et al.*, Phys. Rev. B **69** (2004) 165107.

[30] L. Giordano *et al.*, Phys. Rev. B **76** (2007) 075416.

[31] G. Henkelman, A. Arnaldsson, and H. Jónsson, Comp. Mater. Sci. **36** (2006) 354.

[32] S. Grimme *et al.*, J. Chem. Phys. **132** (2010) 154104.

[33] D. Sun, and W. Li, Chinese J. Catal. **34** (2013) 973.

SCHEMATIC 1. The construction of triangular FeO_x NCs with CUF and CUO edges from monolayer FeO(111) slab. Orange and purple spheres, O and Fe atoms.

FIG. 1. Magnetic structures of the triangular FeO_x NCs: Fe_3O (a), Fe_6O_3 (b), $Fe_{10}O_6$ (c), $Fe_{15}O_{10}$ (d), $Fe_{21}O_{15}$ (e), $Fe_{28}O_{21}$ (f). Orange spheres, O atoms; purple and light blue spheres, Fe atoms with opposite magnetization.

FIG 2. Configurations and stabilities of the FeO_x NCs on Pt(111) with CUF edge. DFT-optimized configurations and relative total energies (ΔE_{tot}) for Fe_3O (a-d), Fe_6O_3 (e-h), $Fe_{10}O_6$ (i-l). In each line, the leftmost configuration is adopted as the energy reference. Orange, purple and dark blue spheres, O, Fe and Pt atoms.

FIG. 3. Configurations and stabilities of the FeO_x NCs on Pt(111) with CUO edge. DFT-optimized configurations and relative total energies (ΔE_{tot}) for Fe_3O_3 (a-b), Fe_3O_6 (c-d), Fe_6O_7 (e-f), Fe_6O_{10} (g-h), $Fe_{10}O_{12}$ (i-j), $Fe_{10}O_{15}$ (k-l). For each NC, the left configuration is adopted as the energy reference. Orange and white spheres, upper and lower O atoms; purple and dark blue spheres, Fe and Pt atoms. For each NC, Fe and O near corner site may deviate their original position.

FIG. 4. Stable configurations of the FeO_x NCs on Pt(111). DFT-optimized configurations for $Fe_{15}O_{10}$ (a), $Fe_{15}O_{21}$ (b), $Fe_{21}O_{15}$ (c), $Fe_{21}O_{28}$ (d), $Fe_{28}O_{21}$ (e), $Fe_{28}O_{36}$ (f). Orange and white spheres; upper and lower O atoms; purple and dark blue spheres, Fe and Pt atoms.

FIG. 5. Contour plots for the distance between adjacent Fe (l_{Fe} in Å) in Fe_3O (a), Fe_6O_3 (b), $Fe_{10}O_6$ (c), $Fe_{15}O_{10}$ (d), $Fe_{21}O_{15}$ (e), $Fe_{28}O_{21}$ (f), Fe_3O_6 (g), Fe_6O_{10} (h), $Fe_{10}O_{15}$ (i), $Fe_{15}O_{21}$ (j), $Fe_{21}O_{28}$ (k), $Fe_{28}O_{36}$ (l) NCs supported on Pt(111). The color scales above and below are for (a-f) and (g-l) respectively. The positions of Fe are given by the hollow dots and the centers of the two adjacent Fe are marked with crosses. At the position of the cross, the color represents the value of the corresponding l_{Fe} while colors in other area are filled via smoothing.

FIG. 6. Contour plots for the relative height of Fe (Δh_{Fe} in Å) in Fe_3O (a), Fe_6O_3 (b), $Fe_{10}O_6$ (c), $Fe_{15}O_{10}$ (d), $Fe_{21}O_{15}$ (e), $Fe_{28}O_{21}$ (f), Fe_3O_6 (g), Fe_6O_{10} (h), $Fe_{10}O_{15}$ (i), $Fe_{15}O_{21}$ (j), $Fe_{21}O_{28}$ (k), $Fe_{28}O_{36}$ (l) NCs supported on Pt(111). The color scale above and below are for (a-f) and (g-l) respectively. The positions of Fe are given by the hollow dots. At the position of the hollow dots, the color represents the value of the corresponding Δh_{Fe} while colors in other area are filled via smoothing.

FIG. 7. Contour plots for the normalized oxidation state of Fe in Fe_3O (a), Fe_6O_3 (b), $Fe_{10}O_6$ (c), $Fe_{15}O_{10}$ (d), $Fe_{21}O_{15}$ (e), $Fe_{28}O_{21}$ (f), Fe_3O_6 (g), Fe_6O_{10} (h), $Fe_{10}O_{15}$ (i), $Fe_{15}O_{21}$ (j), $Fe_{21}O_{28}$ (k), $Fe_{28}O_{36}$ (l) NCs supported on Pt(111). The color scale above and below are for (a-f) and (g-l) respectively. The positions of Fe are given by the hollow dots. At the position of the hollow dots, the color represents the value of the corresponding oxidation state while colors in other area are filled via smoothing.

AIP Publishing
The Journal of Chemical Physics
ACCEPTED MANUSCRIPT

PLEASE CITE THIS ARTICLE AS DOI: 10.1063/1.5129266

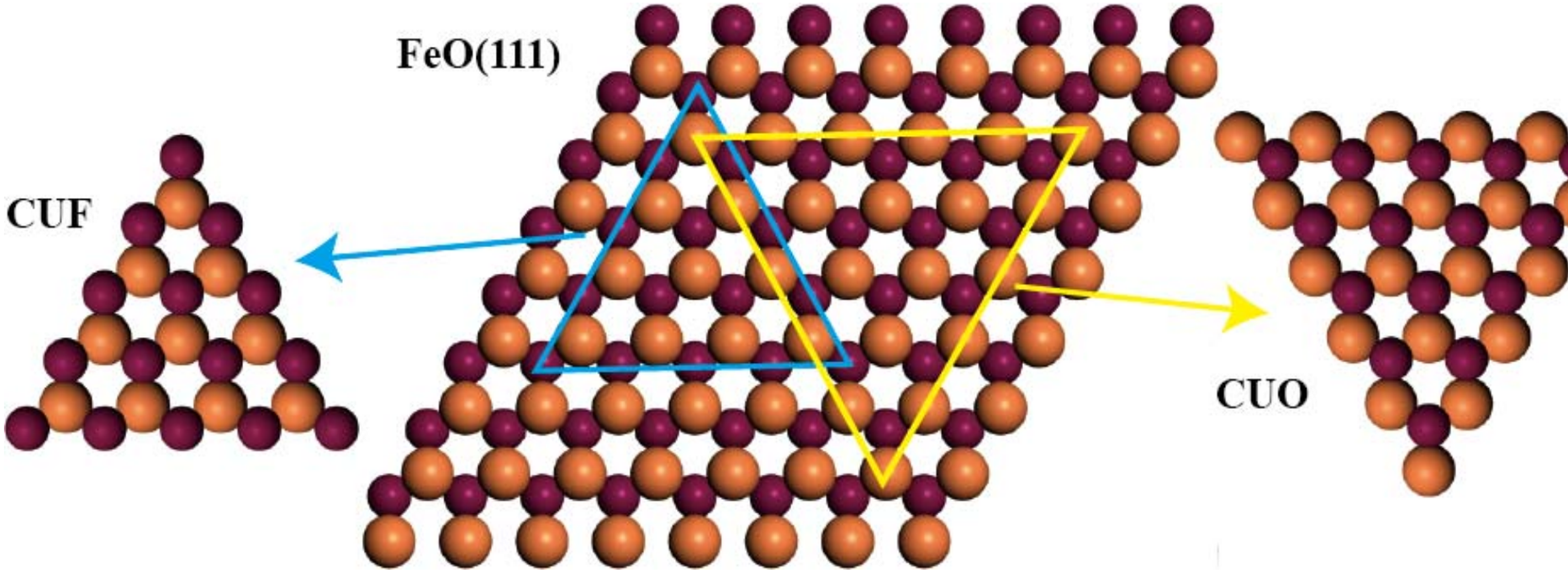

Scheme 1

AIP Publishing
The Journal of Chemical Physics
ACCEPTED MANUSCRIPT

PLEASE CITE THIS ARTICLE AS DOI: 10.1063/1.5129266

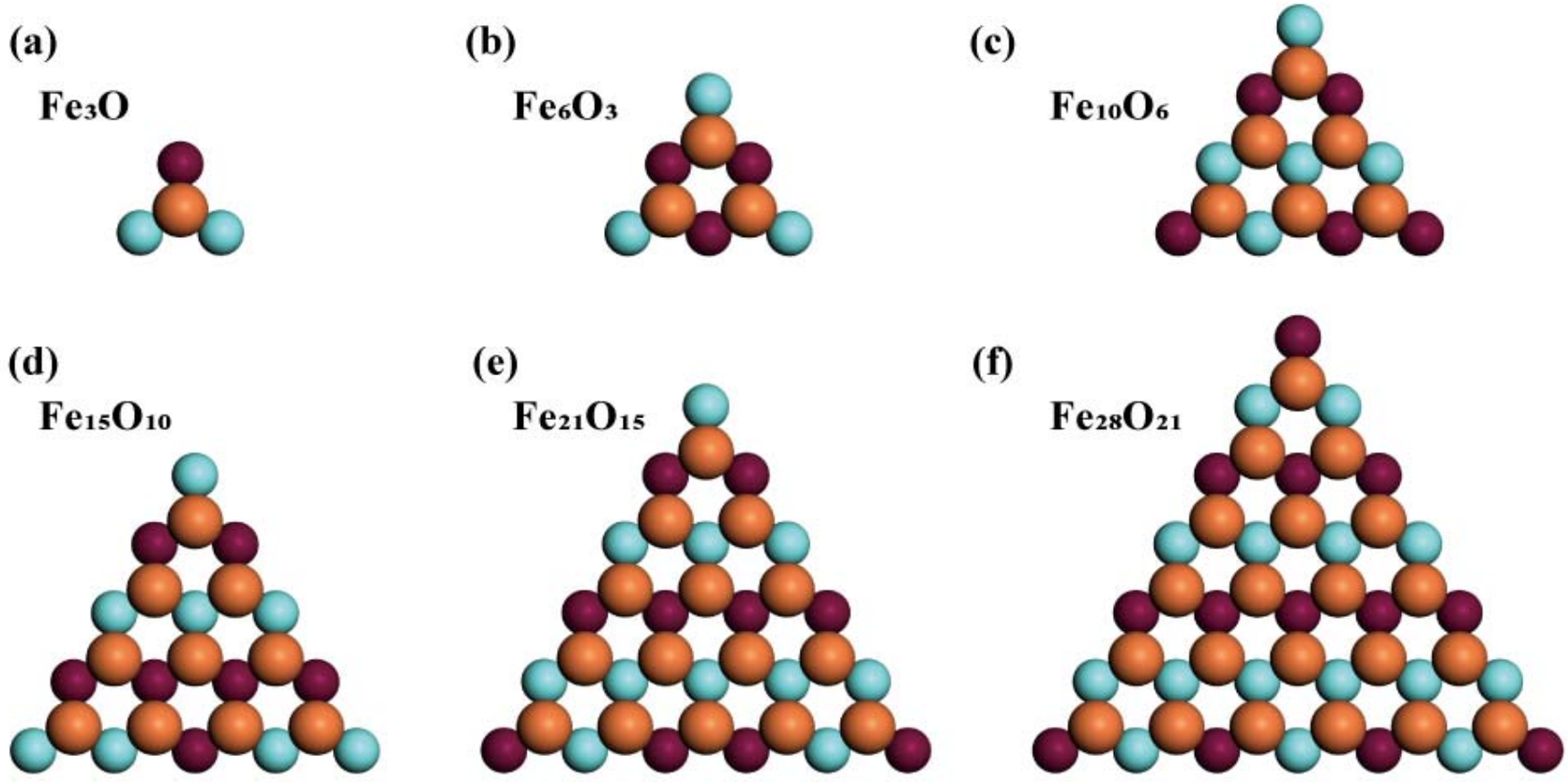

Figure 1

AIP Publishing

The Journal of Chemical Physics

ACCEPTED MANUSCRIPT

This is the author's peer reviewed, accepted manuscript. However, the online version of record will be different from this version once it has been copyedited and typeset.
PLEASE CITE THIS ARTICLE AS DOI: 10.1063/1.5129266

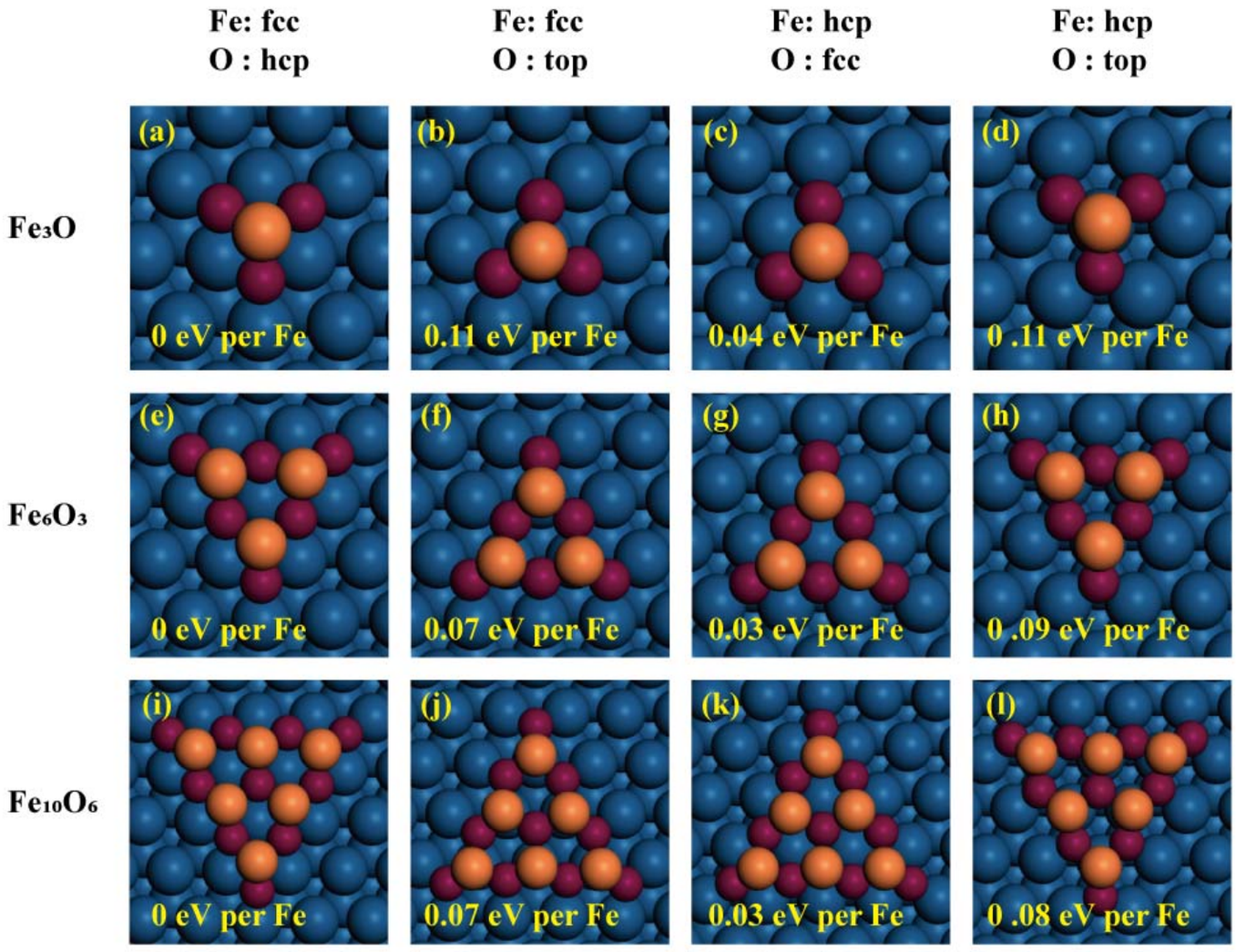

Figure 2

AIP Publishing

The Journal of Chemical Physics

ACCEPTED MANUSCRIPT

PLEASE CITE THIS ARTICLE AS DOI: 10.1063/1.5129266

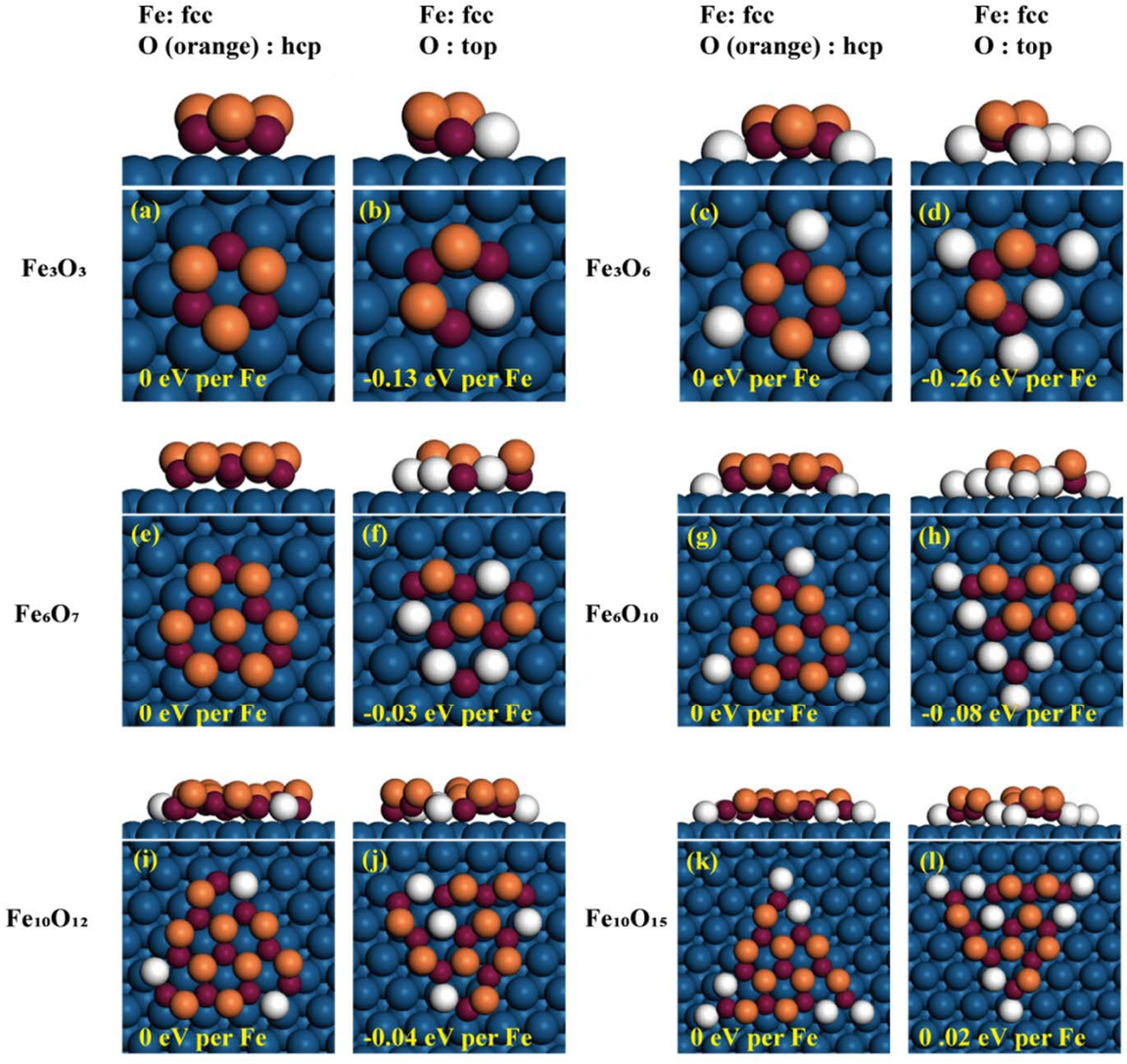

Figure 3

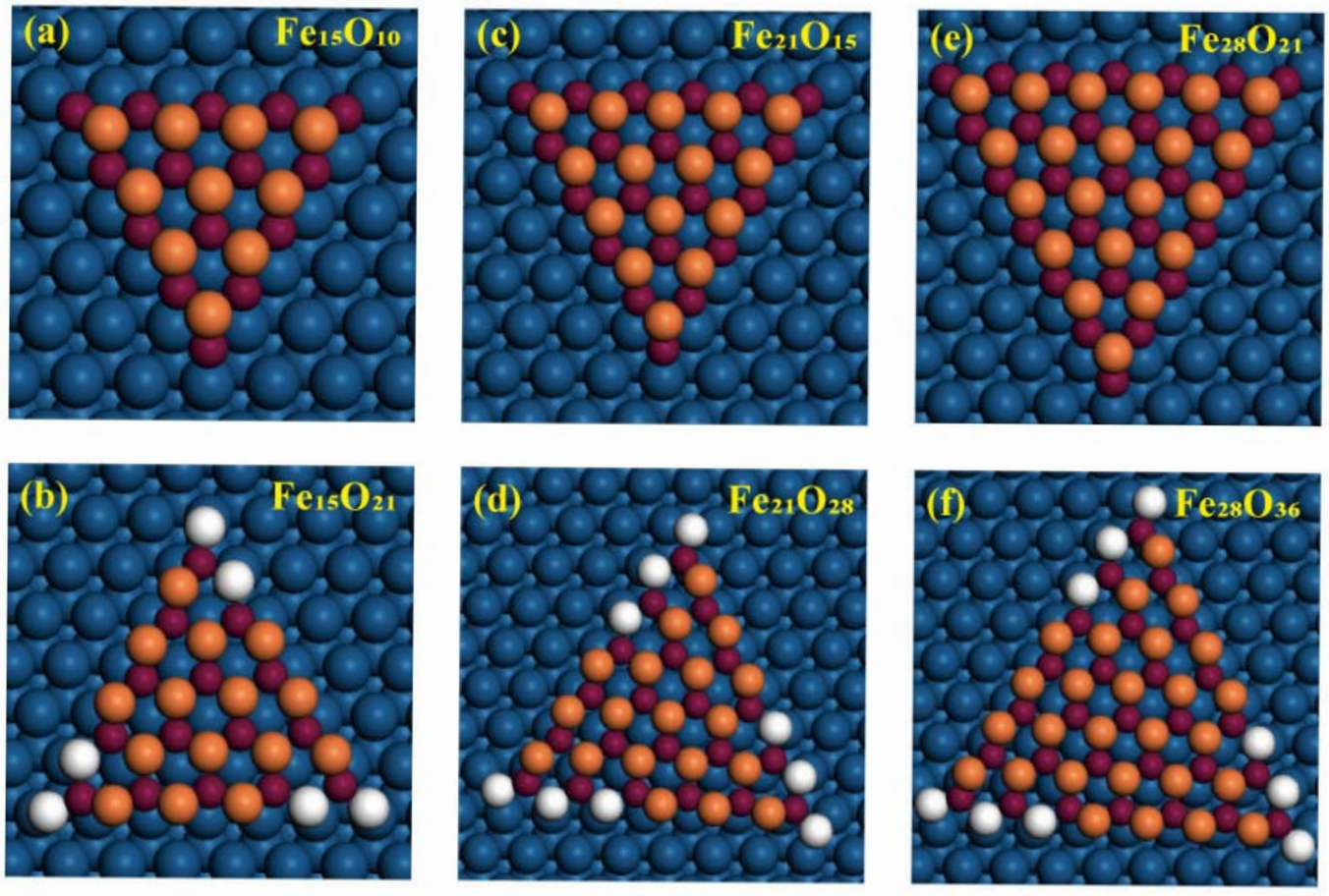

Figure 4

AIP Publishing

The Journal of Chemical Physics

ACCEPTED MANUSCRIPT

PLEASE CITE THIS ARTICLE AS DOI: 10.1063/1.5129266

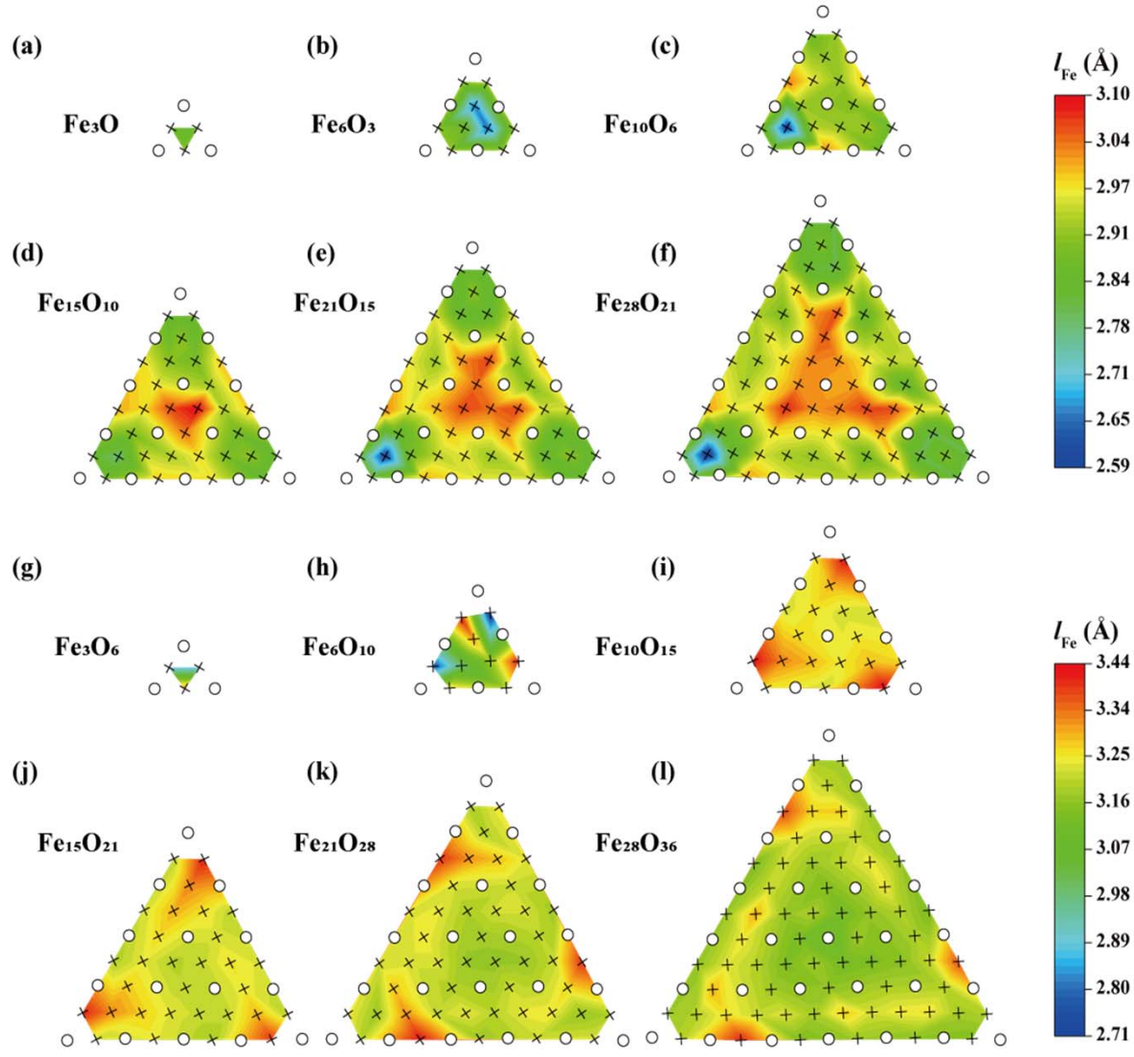

Figure 5

AIP Publishing
The Journal of Chemical Physics
ACCEPTED MANUSCRIPT

PLEASE CITE THIS ARTICLE AS DOI: 10.1063/1.5129266

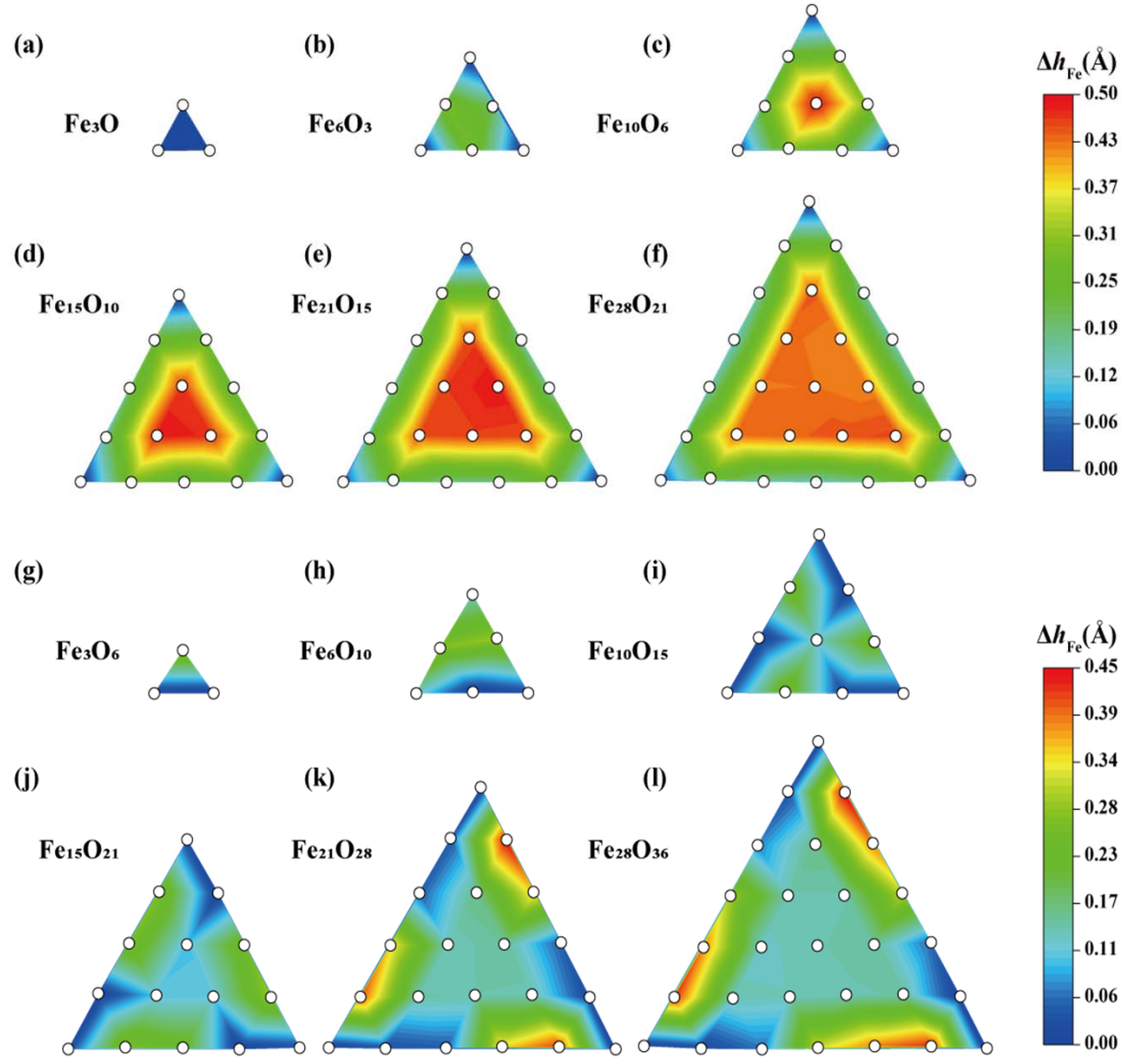

Figure 6

AIP Publishing
The Journal of Chemical Physics
ACCEPTED MANUSCRIPT

PLEASE CITE THIS ARTICLE AS DOI: 10.1063/1.5129266

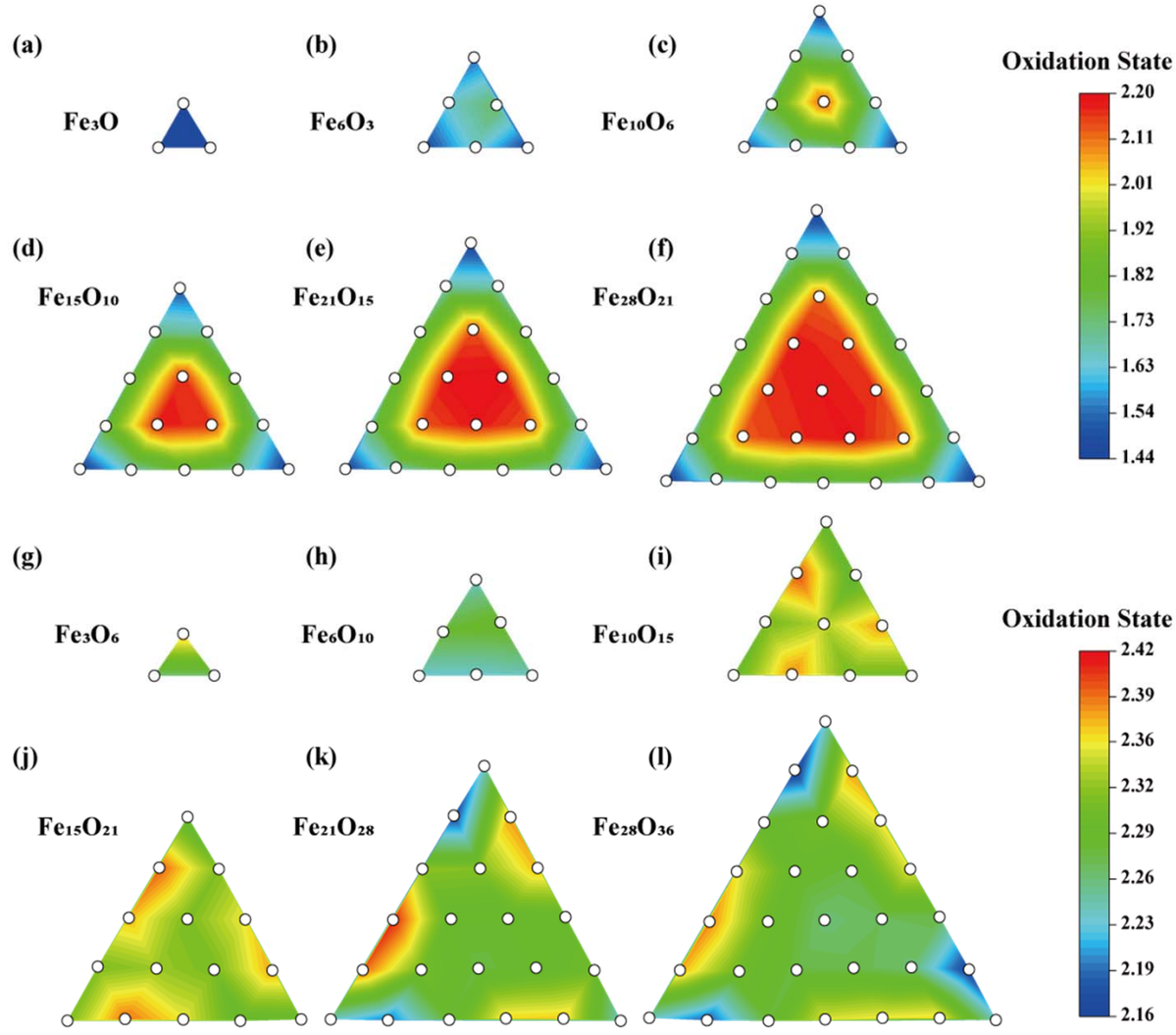

Figure 7